Available online at www.sciencedirect.com
ScienceDirect
Nuclear Medicine and Biology 34 (2007) 681–689
NUCLEAR MEDICINE — AND — BIOLOGY
www.elsevier.com/locate/nucmedbio

Brain and whole-body imaging in nonhuman primates with [^{11}C]MeS-IMPY, a candidate radioligand for β-amyloid plaques☆

Nicholas Seneca*, Lisheng Cai, Jeih-San Liow, Sami S. Zoghbi, Robert L. Gladding, Jinsoo Hong, Victor W. Pike, Robert B. Innis

Molecular Imaging Branch, National Institute of Mental Health, National Institutes of Health, Bethesda, MD 20892-2035, USA

Received 4 April 2007; received in revised form 17 May 2007; accepted 6 June 2007

Abstract

[^{11}C]MeS-IMPY ([*S*-methyl-^{11}C]*N*,*N*-dimethyl-4-(6-(methylthio)imidazo[1,2-*a*]pyridine-2-yl)aniline) is a potential radioligand for imaging β-amyloid plaques with positron emission tomography (PET). The aims of this study were to evaluate [^{11}C]MeS-IMPY uptake in nonhuman primate brain and to estimate radiation exposure from serial whole-body images. Eight PET studies were performed in rhesus monkeys to measure the brain uptake and washout of [^{11}C]MeS-IMPY. Time–activity data were analyzed with one-tissue and two-tissue compartmental models using radiometabolite-corrected plasma input function. In addition, two whole-body PET scans were acquired for 120 min to determine the biodistribution of [^{11}C]MeS-IMPY. Tomographic PET images were compressed into a single planar image to identify organs with the highest radiation exposures. Estimates of the absorbed dose of radiation were calculated using OLINDA 1.0. Injection of [^{11}C]MeS-IMPY caused little change in pulse rate, blood pressure, respiratory rate and temperature. [^{11}C]MeS-IMPY showed high standardized brain uptake values of ~500% and 600% between 2 and 3 min in cortical regions and the cerebellum, respectively. The brain uptake of [^{11}C]MeS-IMPY was widespread and quite uniform across all cortical regions. Activity rapidly washed out of the brain, with 20% of peak activity remaining at 40 min. Thus, all brain regions showed minimal retention of radioactivity, consistent with these healthy young animals having negligible amyloid plaques. Regional brain activity fitted well into a one-tissue compartment model. The average volume of distribution in all brain regions was 7.66±2.14 ml/cm^3 (n=4). The organs with the highest radiation exposure (μSv/MBq) were the gallbladder wall (33.4), urinary bladder (17) and lungs (12.9), with a resulting effective dose of 4.9 μSv/MBq (18 mrem/mCi). The high brain uptake, rapid washout and quantifiable volume of distribution in nonhuman primate brain further support the evaluation of [^{11}C]MeS-IMPY. Calculated dosimetry results are comparable with those for other ^{11}C-labeled brain imaging radioligands.
Published by Elsevier Inc.

Keywords: Positron emission tomography; β-Amyloid plaques; [^{11}C]MeS-IMPY; Dosimetry; Kinetic analysis

1. Introduction

Alzheimer's disease (AD) is characterized by the accumulation of β-amyloid plaques and neurofibrillary tangles containing hyperphosphorylated τ proteins in the brain. Selective imaging of amyloid plaques and neurofibrillary tangles would likely be useful in understanding the pathophysiology of AD, in monitoring its progression and in assessing the efficacy of novel therapies. Several promising in vivo positron emission tomography (PET) radioligands for imaging β-amyloid plaques have been evaluated in both animal models and patients with AD. Brain imaging studies using [^{11}C]PIB(N-methyl-[^{11}C]2-(4-methylaminophenyl)-6-hydroxybenzothiazole), [^{18}F]FDDNP(2-(1-[6-[(2-[^{18}F]fluoroethyl)(methyl)amino]-2-naphthyl]ethylidene)malonitrile), [^{11}C]SB-13([^{11}C])4-N-methylamino-4-hydroxystilbene) and [^{123}I]IMPY(6-iodo-2-(4-dimethylaminephenyl-imidazo[1,2-a]pyridine])) (Fig. 1) have been reviewed elsewhere [1,2]. Briefly, [^{11}C]PIB is the most extensively studied radioligand for imaging β-amyloid plaques in AD patients [3–6]. Both [^{11}C]PIB and [^{11}C]SB-13 share the same binding site and can

☆ Drs. Cai, Pike and Innis are coinventors of [^{11}C]MeS-IMPY. They, along with the National Institutes of Health, could benefit from the licensing of this radioligand.

* Corresponding author. Tel.: +1 301 435 7846; fax: +1 301 480 3610.
E-mail address: nicholasseneca@mail.nih.gov (N. Seneca).

0969-8051/$ – see front matter. Published by Elsevier Inc.
doi:10.1016/j.nucmedbio.2007.06.002

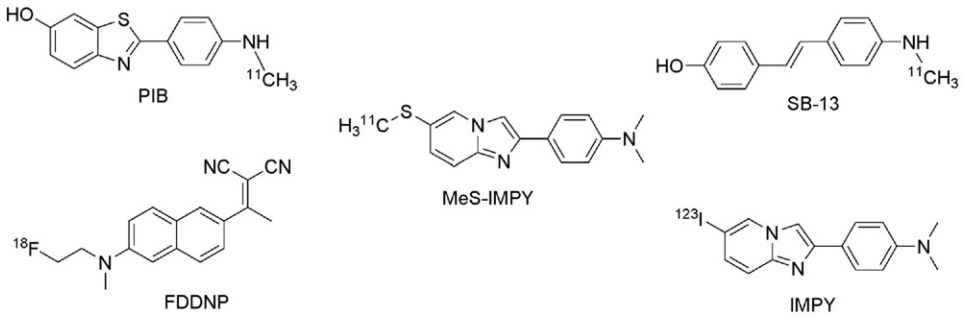

Fig. 1. Structures of [^{11}C]MeS-IMPY, [^{11}C]PIB, [^{18}F]FDDNP, [^{123}I]IMPY and [^{11}C]SB-13.

differentiate patients from healthy age-matched controls [6,7]. [^{18}F]FDDNP binds to both β-amyloid plaques and neurofibrillary tangles [8–10], which is a significant disadvantage since these two proteins have overlapping distributions in the brains of AD patients [11,12]. These radioligands have been shown to be useful, but each suffers from limitations that may inhibit the long-term utility of radioligands. [^{11}C]PIB and [^{11}C]SB-13 have low percentages of specific binding, giving cortex/cerebellum uptake ratios of <2 [4,7], and also have significant uptake in white matter [3,7]. [^{18}F]FDDNP also has a low signal in the brain and is nonselective for β-amyloid plaques over tangles. We seek to develop an improved PET radioligand with greater signal and reduced white matter adsorption.

The aims of the present study were to evaluate the brain uptake of [^{11}C]MeS-IMPY ([*S*-methyl-^{11}C]*N*,*N*-dimethyl-4-(6-(methylthio)imidazo[1,2-*a*]pyridine-2-yl)aniline) with compartmental modeling and to estimate radiation exposure from serial whole-body imaging.

MeS-IMPY showed a high binding affinity to β-amyloid plaques extracted from AD human brains or AD brain homogenates compared to IMPY (K_i=7.93 and 8.95 nM, respectively), while PIB in the same conditions showed a K_i of 7.23 nM (unpublished results). In addition, [^{11}C]MeS-IMPY specifically stained amyloid plaques in human AD cortical brain slices, which was displaced with unlabeled MeS-IMPY (unpublished results). However, binding to neurofibrillary tangles has not been explored, and further studies are needed. The measured log$D_{7.4}$ values for MeS-IMPY and IMPY were 4.1 and 3.58, respectively (unpublished results). It is also selective for β-amyloid plaques, since 10 μM MeS-IMPY caused a <50% inhibition of radioligand binding to a large number of central nervous system receptors (NIMH Pharmacology Drug Screening Program). These receptors included the following: 5-HT1a, 5-HT1b, 5-HT1d, 5-HT1e, 5-HT2a, 5-HT2b, 5-HT2c, 5-HT3 5-HT5a, 5-HT6, 5-HT7, α1a, α1b, α2a, β2, D1, D2, D3, D4, D5, H1 and MOR. In this study, [^{11}C]MeS-IMPY showed high brain uptake and rapid washout, widespread distribution to all cortical regions, slightly higher values of distribution volume in the white matter than in gray matter and stable measurements of distribution volume using one-tissue compartmental analysis. The modest to low radiation exposure would allow multiple PET examinations to be performed on the same subject per year.

2. Materials and methods

2.1. Radiosynthesis of [^{11}C]MeS-IMPY

[^{11}C]MeS-IMPY was prepared by *S*-^{11}C-methylation of a synthesized precursor (methyl 3-(2-(4-(dimethylamino)phenyl)imidazo[1,2-*a*]pyridin-6-ylthio)propanoate). Briefly, [^{11}C]iodomethane was produced with a PET TRACE apparatus (GE Healthcare) via the catalytic reduction of cyclotron-produced [^{11}C]CO_2 to [^{11}C]methane and subsequent gas-phase iodination [13]. In a typical procedure, a precursor and *tert*-butylimino-tris(dimethylamino)phosphorane in anhydrous acetonitrile were treated with [^{11}C]methyl iodide at 80°C for 5 min, and the product was purified by high-performance liquid chromatography [HPLC; Luna C_{18} 5-μm column, 250×10 mm (Phenomenex); mobile phase, 0–2 min, 20% acetonitrile and 80% phosphoric acid (0.1% wt/vol), and then acetonitrile increased linearly to 50% over 15 min; flow rate, 6 ml/min; detection by absorbance at 350 nm; $t_{R\ product}$=9.2 min, $t_{R\ precursor}$=10.5 min]. An HPLC eluate was neutralized with aqueous $NaHCO_3$ solution (8.4% wt/vol; 0.2 ml) and taken to dryness by rotary evaporation at 80°C. The residue of purified [^{11}C]MeS-IMPY was formulated in sterile saline for injection, United States Pharmacopeia (USP) (0.9% wt/vol; 10 ml) plus polysorbate 80 (20 mg), and USP ethanol (0.9 ml), and then passed through a sterile filter into a sterile and pyrogen-free dose vial. The decay-corrected radiochemical yield of [^{11}C]MeS-IMPY was 10−15% from [^{11}C]CO_2, and its specific radioactivity ranged from 1.0 to 4.0 Ci/μmol. Analysis by HPLC showed batches of [^{11}C]MeS-IMPY having a >98% radiochemical purity and being radiochemically stable.

2.2. Animals

Ten PET studies were performed in five male rhesus monkeys (*Macacca mulatta*) weighing 11.6±3.7 kg [these and subsequent data are expressed as mean±standard

deviation (S.D.)]. The PET studies included baseline PET measurements (n=4) and kinetic quantification of the [^{11}C]MeS-IMPY volume of distribution (V_T), which included arterial blood sampling (n=4) and whole-body PET scans (n=2). For all studies, anesthesia was induced with an injection of ketamine (10 mg/kg, im) and then maintained with 1–2% isoflurane and 98% O_2. Electrocardiogram, body temperature, heart rate and respiration rate were measured throughout the experiment. Body temperature was maintained at 37.0–37.5°C with a forced-air heated air blanket. [^{11}C]MeS-IMPY was administered over ~60 s, with injected activity of 191±75 MBq (n=10) and specific activity of 143±145 GBq/μmol (n=10).

Arterial blood was collected in heparin-treated syringes from two monkeys at 15, 30, 45, 60, 75, 90 and 105 s and at 2, 3, 5, 10, 15, 30, 45, 60 and 90 min. The plasma parent radioligand was separated from radiometabolites, as previously described [14]. Whole-blood radioactivity was quantified simultaneously with plasma, which was used for vascular correction in the brain. The plasma free fraction (f_P) of [^{11}C]MeS-IMPY was determined by ultrafiltration with Amicon Centrifree® units, as previously described [15]. The clearance of the area under the curve from zero time to peak activity was calculated using the trapezoid method, and PMOD software (PMOD Technologies Ltd., Adliswil, Switzerland) was used to generate a biexponential fit for all data after the peak.

The injected mass dose of [^{11}C]MeS-IMPY was 0.77±0.53 μg (n=10) in animals with an average body weight of ~12 kg, corresponding to about 0.06 μg/kg. The injection of [^{11}C]MeS-IMPY appeared to be pharmacologically safe in nonhuman primates. The differences between the mean baseline vital sign value and any measurement after the injection of the radioligand was <33 mmHg for systemic blood pressure, <11 min^{-1} for pulse rate, <5 min^{-1} for respiratory rate and <0.7°C for temperature.

2.3. PET data acquisition

2.3.1. Brain imaging

We measured radioactivity in monkey brain with the High-Resolution Research Tomograph (Siemens/CPS, Knoxville, TN, USA). A 6-min transmission scan for attenuation correction was collected using a ^{137}Cs rod source. Emission data for [^{11}C]MeS-IMPY brain studies were collected continuously for 90 min in a list mode. Data were rebinned into 27 dynamic frames of 6×30 s, followed by frames of 3×1, 2×2 and 16×5 min at the time of reconstruction.

Each monkey had a T_1-weighted magnetic resonance imaging (MRI) scan on a GE Signa 1.5-T scanner (spoiled gradient recalled; T_R/T_E/flip angle=13.1 ms/5.8 ms/45°; 0.4×0.4×1.5 mm^3 with coronal orientation on a 256×256×60 matrix).

PET and MRI images were coregistered with PMOD. Six regions of interest were manually defined on summed coronal PET images from 30 min up to the end of the study, with reference to animals' coregistered MRI and brain MRI atlas [16]. Regions of interest were defined on the frontal, parietal, temporal and occipital cortices, the cerebellum and the white matter (centrum semiovale; white matter core of the cerebral hemispheres). Brain uptake was expressed as a standardized uptake value (% SUV), which normalizes for injected activity and body weight: (% injected activity/cm^3 tissue)×(g body weight).

2.3.2. Whole-body imaging

Whole-body transmission and emission scans were acquired on a GE Advance tomograph (GE Medical Systems, Wisconsin). Before radioligand injection, an 8-min transmission scan, using a ^{68}Ge rod source, was obtained on four segments of 15 cm each (the axial field of view of the GE Advance scanner) from the head to the upper thigh. Two male rhesus monkeys (5.3 and 6.0 kg) underwent whole-body PET scans after intravenous injections of 250 and 368 MBq of [^{11}C]MeS-IMPY via the posterior tibial vein. The total scanning time was ~120 min (4×15 s, 4×30 s, 8×1 min, 4×2 min and 2×4 min for each of the four segments of the body from the head to the middle thigh).

2.4. Image analysis

2.4.1. Brain

Time–activity data were analyzed with both one-tissue and two-tissue compartmental models [17] using metabolite-corrected plasma input function. The relationship between parameter estimates and scan duration was analyzed in four PET studies with increasingly truncated data sets from 0 to 90 min to from 0 to 20 min. Goodness of fit by nonlinear squares analysis was evaluated with the Akaike information criterion (AIC) [18] and compared for one-tissue and two-tissue compartment models with F statistics [19]. The identifiability (i.e., standard error) of V_T was calculated from a covariance matrix using the generalized form of error propagation equation [20], where correlations among parameters were taken into account. Identifiability was expressed as percent COV, defined as standard error divided by the value of the parameter (e.g., V_T). Vascular correction was performed using the concentration of radioactivity in whole blood and assuming that blood occupies 5% of brain volume.

The nomenclature (e.g., V_T and f_P) in this article follows that recently recommended by an international group of modeling experts [21].

2.4.2. Whole body

Tomographic PET images were compressed into a single planar image and analyzed with PMOD. Regions of interest were drawn on source organs that could be identified: brain, heart, liver, gallbladder, lungs, kidneys and urinary bladder.

At each time point, decayed activities of identifiable source organs were converted into the fraction of total injected activity. The area under the curve of each organ

was calculated by the trapezoidal method up to the termination of acquisition (120 min). The area after the last image to infinity was calculated by assuming that further decline in radioactivity occurred by physical decay only, without any biologic clearance. The area under the curve of percent injected activity from Time 0 to infinity (after multiplication by 100) is equivalent to the residence time of the organ. Corresponding residence times for a 70-kg man were calculated by a factor to correct for organ and body weights: $(b_m/o_m)(b_h/o_h)$, where b_m and b_h are the body weights of monkeys and humans, respectively, and o_m and o_h are the organ weights of monkeys and humans, respectively.

The mean cumulative urine activities of two monkeys were fitted with a biexponential curve to estimate the percentage of injected activity excreted via this route. The dynamic bladder model (with a 2.4-h voiding interval) was implemented in OLINDA/EXM 1.0 to calculate organ absorbed doses [22]. A voiding interval of 4.8 h had minimal effects on estimated radiation doses, as expected for the short half-life of ^{11}C (20 min).

The organ values of injected activity were corrected for the recovery of measured activity. To accomplish this, a large region of interest was placed over the entire body for each of the 22 frames. The injected activity of each source organ at every time point was corrected for recovery by multiplying by $100/X$, where X is the measured recovery for an individual frame. The average recovery of all frames in both monkeys was ~91%. If no radioactivity is lost to excretion, the total of all residence times equals $T_{1/2}/\ln 2$, where $T_{1/2}$=20.4 min=0.34 h. Thus, the total should equal 0.49 h. The residence time of the "remainder of the body" for each animal was calculated as 0.49 minus the sum of the residence times of source organs.

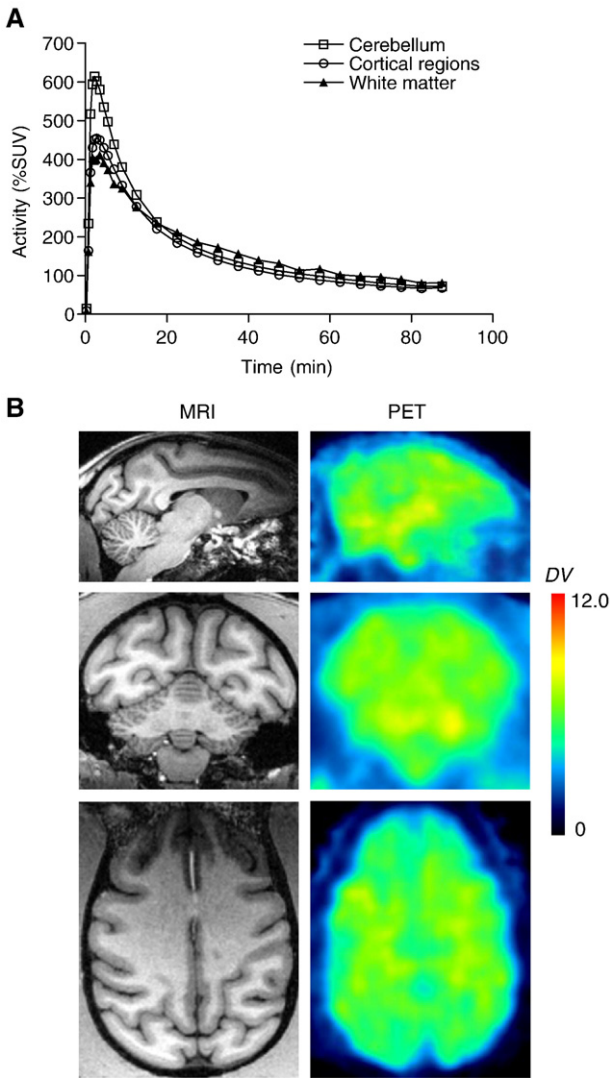

Fig. 2. (A) Average time course of the regional rhesus brain activity of [^{11}C]MeS-IMPY (mean; n=6). Bars for S.D. were not included because of inadequate spaces between curves. As a measure of differences among studies, the average coefficient of variation (S.D./mean) for the cerebellum was 18% for the peak value at 2 min and 37% for the value at 80 min. (B) PET images of [^{11}C]MeS-IMPY estimated by the one-tissue compartment model in rhesus brain. Parametric images of V_T (ml/cm^3) are presented on the right. The corresponding monkey 4.7-T MRI (on the left) was used for a clearer representation of anatomic areas. MRI was performed with a vertical 4.7-T (Bruker Medical) scanner with a 40-cm bore. The monkey was imaged with a standard head coil fitted to accommodate the size of the monkey.

3. Results

3.1. Brain uptake of [^{11}C]MeS-IMPY

After intravenous administration of [^{11}C]MeS-IMPY, brain uptake was high in cortical regions (frontal, parietal, temporal and occipital cortices) and the cerebellum (454±8.1% and 614±109% SUV; n=6), with lower peak levels in the white matter (411±129% SUV; Fig. 2A and B). The distribution of brain uptake for [^{11}C]MeS-IMPY was widespread and fairly uniform in all cortical brain regions. Brain activity peaked early and washed out quickly. Uptake in cortical regions decreased slightly more rapidly than that in the white matter by 40 min to approximately 120%, compared to 150% SUV, respectively.

3.2. Arterial plasma analysis

The plasma activity of [^{11}C]MeS-IMPY peaked at about 1 min and decreased rapidly to 21% and 2% of that value by 2 and 10 min, respectively (Fig. 3A). [^{11}C]MeS-IMPY was quickly metabolized and represented 86±9%, 66±19%, 7±1% and 4±1% of total plasma activity at 1, 2, 15 and 30 min, respectively (Fig. 3B). Three radiometabolites were detected in all 57 arterial plasma samples. The most polar Radiometabolite A eluted at the column void volume with a retention time of 2.2±0.3 min, followed by Radiometabolite B (3.5±0.6 min) and Radiometabolite C (4.8±0.6 min), with the parent radioactive peak occurring at 6.6±0.8 min. All radiometabolites were less lipophilic than the parent compound. The free fraction (f_P) of radioligand in plasma was similar between monkeys (0.83±0.17; n=3). [^{11}C]MeS-

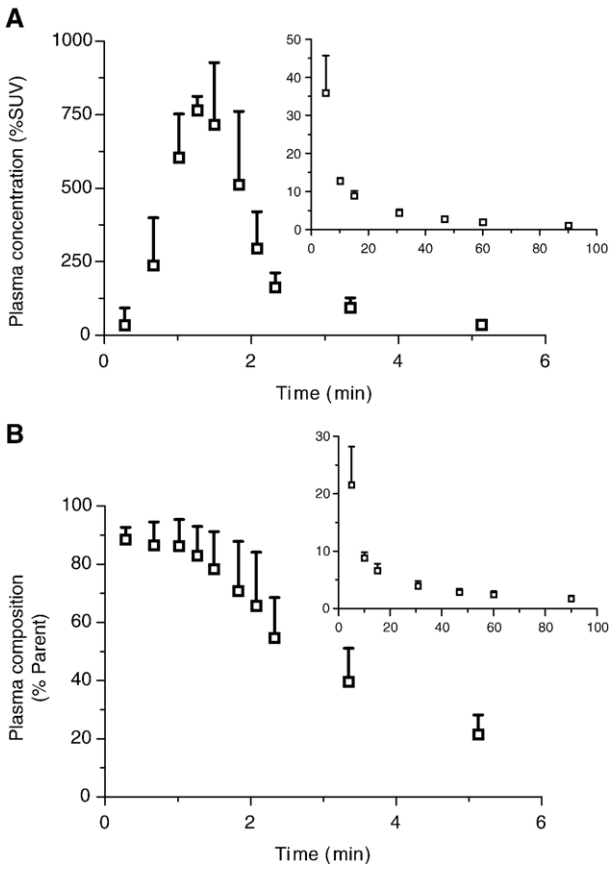

Fig. 3. (A) [^{11}C]MeS-IMPY plasma concentration after radioligand injection. The curve is shown with two time intervals (0–6 and 6–100 min) because of high concentrations at early time points. Symbols represent the mean±S.D. (n=4), although the S.D. was sometimes less than the size of the symbol. (B) Parent composition of plasma. Values are presented as the percentage of total plasma radioactivity of the parent ligand [^{11}C]MeS-IMPY. Symbols represent mean±S.D. (n=4).

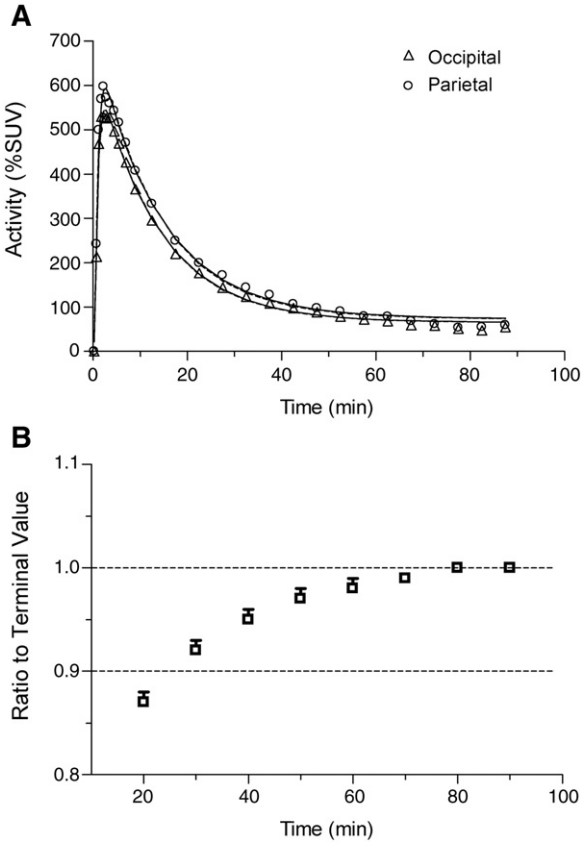

Fig. 4. (A) Fitting of one-tissue compartment analysis (dashed line). (B) Time stability of V_T determined from the one-tissue compartment model. Each point represents the mean±S.D. (n=4) of all regions (frontal, parietal, temporal and occipital cortices and the cerebellum) analyzed with data from Time 0 to the specified time and expressed as the percentage of the 90-min value.

IMPY was rapidly removed from arterial plasma, with a clearance of 693±234 ml/min.

3.3. Compartmental analysis

Convergence was achieved in all regions and all animals (n=4) with one-tissue and two-tissue compartmental models (Fig. 4A). AIC values were lower for the two-tissue compartment model (108±20.1) than for the one-tissue compartment model (143.2±23.5), but this difference was not significant by F test in all regions of all animals (P<.25). Because the two-tissue model was not statistically superior to the one-tissue model, subsequent analysis used the simpler one-tissue model. The total distribution volume V_T includes both specific free and nonspecifically bound activities in the brain. V_T was well identified using the one-tissue compartment model, showing a % COV of 4.96±1.65. The one-tissue compartment model estimate for all regions and all monkeys was 7.66±2.14 ml/cm^3 (n=4). The time stability of parameter estimation was analyzed for the frontal, parietal, temporal and occipital cortices and the cerebellum. V_T was identified

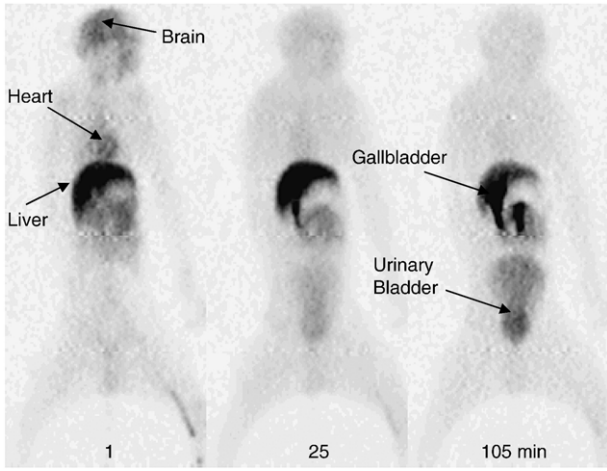

Fig. 5. Whole-body images at 1, 25 and 105 min after the injection of [^{11}C]MeS-IMPY. [^{11}C]MeS-IMPY was administered over 60 s, with an injected activity of 250 MBq. Anesthesia was induced with the injection of ketamine (10 mg/kg IM) and then maintained with 1–2% isoflurane and 98% O_2.

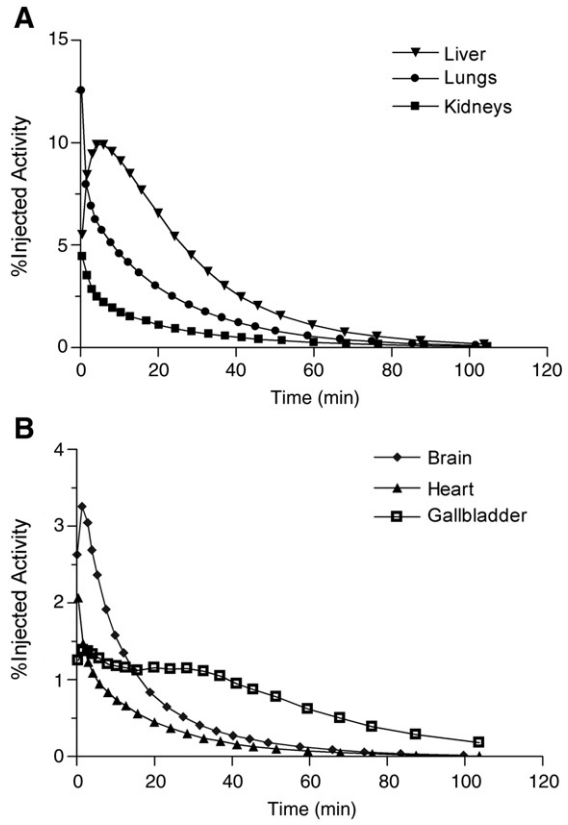

Fig. 6. Mean organ uptake in the (A) liver, lungs and kidneys; and (B) brain, heart and gallbladder. An organ's decayed activity is expressed as a percentage of injected activity.

quickly, was stable for all regions and had a <10% change between 30 and 90 min by one-tissue compartmental analysis (Fig. 4B). The early identification of V_T suggests a rapid achievement of steady-state concentrations of radioligands in the brain and plasma. The quite stable values of V_T from 30 to 90 min were consistent with, but do not prove, the absence of significant concentrations of radiometabolites in the brain.

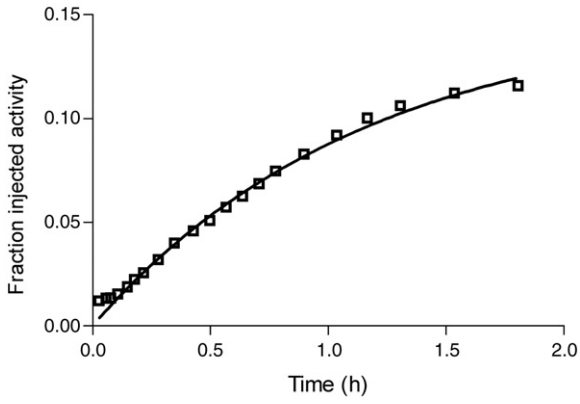

Fig. 7. Decay-corrected activity curve overlying the urinary bladder after [^{11}C]MeS-IMPY injection. Data are presented as the average of two monkeys and are expressed as percentages of injected activity. The solid line is the biexponential fit of data points (□), and its asymptote implies that 15% of injected activity will be excreted via urine at infinite time.

Table 1
Human residence times for [^{11}C]MeS-IMPY extrapolated from the average of two rhesus monkeys

Organ	Residence time (h)		
	Monkey 1	Monkey 2	Average
Brain	0.008	0.017	0.012
Heart	0.005	0.030	0.004
Liver	0.038	0.074	0.056
Gallbladder	0.012	0.014	0.013
Lungs	0.053	0.040	0.047
Kidneys	0.016	0.007	0.012
Bladder	0.025	0.017	0.021
Remainder of the body	0.333	0.319	0.326

The residence time of the "remainder of the body" was calculated such that the sum of all residence times in each animal equals $T_{1/2}$/ln2=0.34 h/ln2=0.49 h.

3.4. Whole-body dosimetry

The brain, heart, liver, gallbladder, lungs, kidneys and urinary bladder were visually identified as organs with moderate to high activities (Fig. 5). Uptake of radioactivity was highest in the lungs, with a peak of 12% injected activity at the first frame acquisition. Peak values of activity in the brain, heart, liver, gallbladder and kidneys were 3.2%, 2.1%, 9.9%, 1.3% and 4.5% of injected activity, respectively, and all occurred within 6 min (Fig. 6A and B).

The average cumulative urine activity fitted well (r^2=.993) with a biexponential curve, using PRISM version

Table 2
Radiation dosimetry of [^{11}C]MeS-IMPY extrapolated from the mean of two monkeys and estimated for a 70-kg human male

Target organ	μSv/MBq	mrem/mCi
Adrenal glands	3.4	12.4
Brain	3.2	11.9
Breasts	2.1	7.9
Gallbladder wall	33.4	123.5
Lower large intestinal wall	2.7	9.9
Small intestine	2.8	10.5
Stomach	2.7	10.1
Upper large intestinal wall	2.9	10.9
Heart wall	5.1	18.9
Kidneys	11.7	43.4
Liver	10.7	39.4
Lungs	12.9	47.8
Muscle	2.3	8.6
Ovaries	2.8	10.2
Pancreas	3.4	12.5
Red marrow	2.2	8.2
Osteogenic cells	3.2	11.9
Skin	1.8	6.7
Spleen	2.7	9.9
Testes	2.2	8.1
Thymus	2.5	9.3
Thyroid	2.2	8.2
Urinary bladder wall	17.0	62.9
Uterus	3.1	11.7
Total body	2.8	10.5
Effective dose equivalent	7.7	28.4
Effective dose	4.9	18.0

4.0 software (GraphPad Software) (Fig. 7). Exponential fitting implied that an asymptote of ~15% of injected activity was excreted via urine by time infinity.

Human residence times were extrapolated from planar images using the average values of the two monkeys (Table 1). Radiation absorbed dose estimates were calculated with the OLINDA/EXM 1.0 computer program, with a urine-voiding interval of 2.4 h (Table 2). The organs with the highest radiation burden (μSv/MBq) were the gallbladder (33.4), urinary bladder wall (17), lungs (12.90) and kidneys (11.73). The effective dose was estimated to be 4.9 μSv/MBq, with a 2.4-h voiding interval (Table 2).

4. Discussion

4.1. Summary

[^{11}C]MeS-IMPY showed several promising characteristics in monkeys enough for such PET radioligand to image β-amyloid plaques in human subjects. Brain uptake corrected for vascular radioactivity was high (~500–600% SUV) and peaked quickly (~2–3 min). Thereafter, activity washed out rapidly, with ~70% of peak values eliminated by 30 min. Large delivery to the brain and fast washout are desirable for a radioligand in animals that lack a receptor target. The rhesus monkeys in this study were 5–10 years of age and were expected to be virtually devoid of β-amyloid deposits [23]. In humans with significant amyloid deposits, a useful radioligand would show the same high delivery to the brain but a much slower washout from regions containing β-amyloid plaques, as it is retained by binding and rebinding to the target.

The brain uptake of [^{11}C]MeS-IMPY was well identified with a one-tissue compartment model as the total distribution volume V_T, which equals the ratio of total radioactivity in the brain to the concentration of the parent radioligand (free plus protein bound) in plasma at equilibrium. Relative to the analysis of all 90-min data, V_T was identified within only the initial 30 min of data to be within 10% of the terminal, a presumably more accurate value. PET measurements of brain activity derive from any ^{11}C chemical form (i.e., [^{11}C]MeS-IMPY plus any radiometabolite in the field of view). In contrast, plasma concentrations represented only the parent radioligand separated from radiometabolites. Since V_T represents the ratio of total brain activity to the plasma concentration of [^{11}C]MeS-IMPY, the relative stability of V_T from 30 to 90 min was consistent with, but does not prove, the absence of a significant percentage of radiometabolites in the brain.

4.2. Comparison with [^{123}I]IMPY and [^{11}C]PIB

IMPY analogs show promise to image β-amyloid plaques in the brain. Both IMPY and MeS-IMPY bind with high affinity (K_i=8.95 and 7.93 nM, respectively [3]) to β-amyloid plaques in postmortem human brain tissues from patients with AD. In preliminary studies, [^{123}I]IMPY has been shown to differentiate AD patients from controls, but retention of the radioligand showed only a ~40% increased binding in patients compared to controls [24].

We cannot directly compare [^{11}C]MeS-IMPY and [^{123}I]IMPY, since imaging in nonhuman primates has not been reported for the latter. Nevertheless, [^{11}C]MeS-IMPY would have the standard advantages and disadvantages of a PET radioligand compared to a single-photon emission computed tomography (SPECT) radioligand. PET has sensitivity and spatial resolution higher than those of SPECT. The short half-life of ^{11}C (20 min) compared to that of ^{123}I (13 h) typically requires local production and an on-site cyclotron. The achievable specific activity of ^{123}I radioligands is typically greater than that of ^{11}C-labeled agents and allows the injection of a smaller mass dose. For example, the reported specific activity of [^{123}I]IMPY was 8806 GBq/μmol, whereas that of [^{11}C]MeS-IMPY in this study was ~143±145 GBq/μmol. The radiation burden of ^{11}C is significantly less than that of ^{123}I. For example, the effective dose of [^{123}I]IMPY was 35.7 μSv/MBq [25], whereas that of [^{11}C]MeS-IMPY was 4.9 μSv/MBq in this study.

[^{11}C]PIB is the most extensively evaluated — and arguably the most promising — PET radioligand to image β-amyloid plaques in the brain [3,5,6,26,27]. [^{11}C]PIB has been studied in nonhuman primates [27], and [^{11}C]MeS-IMPY has shown favorable comparative characteristics in the current study. That is, the brain uptake of [^{11}C]MeS-IMPY was higher and washed out similar to that of [^{11}C]PIB. The peak cortical uptake was ~500% at 2–3 min for [^{11}C]MeS-IMPY and was ~300% SUV at ~10 min for [^{11}C]PIB. The washout of [^{11}C]MeS-IMPY was similar to that of [^{11}C]PIB, since the residual brain activity uptake at 40 min was ~100% SUV for [^{11}C]MeS-IMPY and [^{11}C]PIB. Although this animal model suggests that [^{11}C]MeS-IMPY will perform as well as, if not better than, [^{11}C]PIB, useful comparison must await clinical trials in AD patients with this novel IMPY analog.

A significant limitation of [^{18}F]FDDNP compared to [^{11}C]PIB is that the former binds to both amyloids and tangles, whereas the latter is selective for amyloid plaques at low in vivo concentrations used with PET imaging [28]. MeS-IMPY and PIB have similar chemical structures (Fig. 1). Thus, we expect that MeS-IMPY will also be selective for β-amyloid plaques over τ proteins, but we have not yet examined this important parameter.

4.3. Dosimetry

Serial whole-body PET studies were performed in nonhuman primates to estimate radiation absorbed doses of [^{11}C]MeS-IMPY. The organ with the highest radiation burden was the gallbladder (33.4 μSv/MBq), followed by the urinary bladder, lungs and kidneys. The use of planar images for data analysis provided conservative estimates of radiation exposure, since large regions of interest included

overlying tissues. We previously compared radiation exposure estimated with 2-D planar, bisected and thin-slice tomographic images with the substance P (NK1) receptor radioligand, [^{18}F]SPA-RQ [29]. Planar and bisected images provided organ dose estimates similar to, but slightly higher than, those of thin-slice images.

Whole-body PET imaging of [^{11}C]MeS-IMPY caused moderate to low radiation exposures, with an effective dose of 4.9 μSv/MBq (18.0 mrem/mCi). The effective dose estimate for [^{11}C]MeS-IMPY is comparable to those for other ^{11}C-labeled brain imaging agents such as [^{11}C]PIB (6.5 μSv/MBq) and [^{11}C]acetate (4.9 μSv/MBq) [30,31].

5. Conclusion

In summary, the brain uptake of [^{11}C]MeS-IMPY in nonhuman primates showed promising characteristics as a potential radioligand for imaging β-amyloid plaques. Compared to [^{11}C]PIB, [^{11}C]MeS-IMPY has higher cortical uptake and faster washout in nonhuman primates. Brain uptake was quantifiable relative to serial arterial measurements of [^{11}C]MeS-IMPY. The total distribution volume was identified within 30 min and was relatively stable for the subsequent 60 min. Radiation dosimetry would allow multiple PET scans per year in the same subject due to relatively modest absorbed doses typical of ^{11}C-labeled radioligands.

Acknowledgments

This research was supported by the Intramural Program (project Z01-MH-002795-04) of the National Institute of Mental Health (NIMH). We thank John Bacher, D.V.M., for veterinary care; the staff of the National Institutes of Health PET Department for the successful completion of scanning studies; the NIMH Psychoactive Drug Screening Program (Director Bryan Roth, M.D., Ph.D.; contract NO1MH32004) for measuring the affinity of MeS-IMPY at numerous receptors; and PMOD Technologies Ltd. for providing its image analysis and modeling software.

References

[1] Cai L, Innis RB, Pike VW. Radioligand development for PET imaging of beta-amyloid (Aβ) — current status. Curr Med Chem 2007;14:19–52.
[2] Lockhart A. Imaging Alzheimer's disease pathology: one target, many ligands. Drug Discov Today 2006;11:1093–9.
[3] Klunk WE, Engler H, Nordberg A, Wang Y, Blomqvist G, Holt DP, et al. Imaging brain amyloid in Alzheimer's disease with Pittsburgh Compound-B. Ann Neurol 2004;55:306–19.
[4] Lopresti BJ, Klunk WE, Mathis CA, Hoge JA, Ziolko SK, Lu X, et al. Simplified quantification of Pittsburgh Compound B amyloid imaging PET studies: a comparative analysis. J Nucl Med 2005;46:1959–72.
[5] Mintun MA, Larossa GN, Sheline YI, Dence CS, Lee SY, Mach RH, et al. [^{11}C]PIB in a nondemented population: potential antecedent marker of Alzheimer disease. Neurology 2006;67:446–52.
[6] Price JC, Klunk WE, Lopresti BJ, Lu X, Hoge JA, Ziolko SK, et al. Kinetic modeling of amyloid binding in humans using PET imaging and Pittsburgh Compound-B. J Cereb Blood Flow Metab 2005;25:1528–47.
[7] Verhoeff NP, Wilson AA, Takeshita S, Trop L, Hussey D, Singh K, et al. In-vivo imaging of Alzheimer disease beta-amyloid with [^{11}C]SB-13 PET. Am J Geriatr Psychiatry 2004;12:584–95.
[8] Agdeppa ED, Kepe V, Petri A, Satyamurthy N, Liu J, Huang SC, et al. In vitro detection of (*S*)-naproxen and ibuprofen binding to plaques in the Alzheimer's brain using the positron emission tomography molecular imaging probe 2-(1-[6-[(2-[^{18}F]fluoroethyl)(methyl)amino]-2-naphthyl]ethylidene)malono nitrile. Neuroscience 2003;117:723–30.
[9] Kepe V, Huang SC, Small GW, Satyamurthy N, Barrio JR. Visualizing pathology deposits in the living brain of patients with Alzheimer's disease. Methods Enzymol 2006;412:144–60.
[10] Small GW, Kepe V, Ercoli LM, Siddarth P, Bookheimer SY, Miller KJ, et al. PET of brain amyloid and tau in mild cognitive impairment. N Engl J Med 2006;355:2652–63.
[11] Di Patre PL, Read SL, Cummings JL, Tomiyasu U, Vartavarian LM, Secor DL, et al. Progression of clinical deterioration and pathological changes in patients with Alzheimer disease evaluated at biopsy and autopsy. Arch Neurol 1999;56:1254–61.
[12] Mann DM. The topographic distribution of brain atrophy in Alzheimer's disease. Acta Neuropathol (Berl) 1991;83:81–6.
[13] Schonbachler R, Ametamey S, Schubiger P. Synthesis of ^{11}C-radiolabelling of a tropane derivative lacking the 2 beta ester group: a potential PET-tracer for the dopamine transporter. J Label Compd Radiopharm 1999;42:447–56.
[14] Zoghbi SS, Shetty HU, Ichise M, Fujita M, Imaizumi M, Liow JS, et al. PET imaging of the dopamine transporter with [^{18}F]-FECNT: a polar radiometabolite confounds brain radioligand measurements. J Nucl Med 2006;47:520–7.
[15] Gandelman MS, Baldwin RM, Zoghbi SS, Zea-Ponce Y, Innis RB. Evaluation of ultrafiltration for the free-fraction determination of single photon emission computed tomography (SPECT) radiotracers: beta-CIT IBF, and iomazenil. J Pharm Sci 1994;83:1014–9.
[16] Paxinos G, Huang XF, Toga AW. The rhesus monkey brain in stereotaxic coordinates. San Diego: Academic Press; 2000.
[17] Cunningham V, Lammertsma A. Radioligand studies in brain: kinetic analysis of PET data. Med Chem Res 1995;5:79–96.
[18] Akaike H. A new look at the statistical model identification. IEEE Trans Automat Contr 1974;AC19:716–23.
[19] Hawkins RA, Phelps ME, Huang SC. Effects of temporal sampling, glucose metabolic rates, and disruptions of the blood–brain barrier on the FDG model with and without a vascular compartment: studies in human brain tumors with PET. J Cereb Blood Flow Metab 1986;6:170–83.
[20] Bevington PR, Robinson DK. Data reduction and error analysis for the physical sciences. New York: McGraw-Hill; 2003.
[21] Innis RB, Cunningham V, Delforge J, Fujita M, Gunn RN, Holden J, et al. Consensus nomenclature for in vivo imaging of reversibly binding radioligands. J Cereb Blood Flow Metab 2007 [in press].
[22] Stabin MG, Sparks RB, Crowe E. OLINDA/EXM: the second-generation personal computer software for internal dose assessment in nuclear medicine. J Nucl Med 2005;46:1023–7.
[23] Sani S, Traul D, Klink A, Niaraki N, Gonzalo-Ruiz A, Wu CK, et al. Distribution, progression and chemical composition of cortical amyloid-beta deposits in aged rhesus monkeys: similarities to the human. Acta Neuropathol (Berl) 2003;105:145–56.
[24] Newberg AB, Wintering NA, Plossl K, Hochold J, Stabin MG, Watson M, et al. Use of ^{123}I-IMPY SPECT to differentiate Alzheimer's disease from controls. J Nucl Med 2006;47(220).
[25] Newberg AB, Wintering NA, Plossl K, Hochold J, Stabin MG, Watson M, et al. Safety, biodistribution, and dosimetry of ^{123}I-IMPY: a novel amyloid plaque-imaging agent for the diagnosis of Alzheimer's disease. J Nucl Med 2006;47:748–54.

[26] Klunk WE, Lopresti BJ, Ikonomovic MD, Lefterov IM, Koldamova RP, Abrahamson EE, et al. Binding of the positron emission tomography tracer Pittsburgh compound-B reflects the amount of amyloid-beta in Alzheimer's disease brain but not in transgenic mouse brain. J Neurosci 2005;25:10598–606.

[27] Mathis CA, Wang Y, Holt DP, Huang GF, Debnath ML, Klunk WE. Synthesis and evaluation of ^{11}C-labeled 6-substituted 2-arylbenzothiazoles as amyloid imaging agents. J Med Chem 2003;46:2740–54.

[28] Bacskai BJ, Hickey GA, Skoch J, Kajdasz ST, Wang Y, Huang GF, et al. Four-dimensional multiphoton imaging of brain entry, amyloid binding, and clearance of an amyloid-beta ligand in transgenic mice. Proc Natl Acad Sci U S A 2003;100:12462–7.

[29] Sprague DR, Chin FT, Liow JS, Fujita M, Burns HD, Hargreaves R, et al. Human biodistribution and radiation dosimetry of the tachykinin NK1 antagonist radioligand [^{18}F]SPA-RQ: comparison of thin-slice, bisected, and 2-dimensional planar image analysis. J Nucl Med 2007;48:100–7.

[30] Parsey RV, Sokol LO, Belanger MJ, Kumar JS, Simpson NR, Wang T, et al. Amyloid plaque imaging agent [C-11]-6-OH-BTA-1: biodistribution and radiation dosimetry in baboon. Nucl Med Commun 2005;26:875–80.

[31] Seltzer MA, Jahan SA, Sparks R, Stout DB, Satyamurthy N, Dahlbom M, et al. Radiation dose estimates in humans for ^{11}C-acetate whole-body PET. J Nucl Med 2004;45:1233–6.